Available online at www.sciencedirect.com

SciVerse ScienceDirect

Procedia Engineering 19 (2011) 81 – 87

Procedia Engineering

www.elsevier.com/locate/procedia

1st CIRP Conference on Surface Integrity (CSI)

Kinematic and Stochastic Surface Topography of Machined TiAl6V4-Parts by means of Ball Nose End Milling

B. Denkena, V. Böß, D. Nespor*, A. Samp

Institute of Production Engineering and Machine Tools, Leibniz Universität Hannover
An der Universität 2, 30823 Garbsen, Germany

Abstract

Ball nose end mills are usually applied during 5-axes machining of high functional parts especially in the aerospace industry. The systematical study of the relationship between process forces and kinematics, surface topography and subsurface properties is fundamental to ensure a high surface integrity. This paper deals with the topography of machined surfaces of TiAl6V4 parts by means of ball nose end milling. The machined surface has been analyzed and the kinematic topography, influenced by the process parameters and the geometry of the cutting tool, has been computed. By subtracting the surface measurements from the computed topography, the stochastic topography of the machined surface, e.g. roughness and cracks, can be determined. Furthermore, an approach is given for predicting the stochastic topography based on the process forces during machining of TiAl6V4.

Selection and peer-review under responsibility of Prof. E. Brinksmeier

Keywords: Milling, Topography, Titanium

1. Introduction

Ball nose end mills are commonly used for finishing of sculptured surfaces such as dies, molds or blade and vane airfoil geometries. The machined surface topography is an important aspect of the surface integrity and has a crucial influence on the operational characteristics of such parts. This becomes evident with e.g. gas turbines, which show a significant decrease in their performance when using blades with a high airfoil roughness [1, 2]. Bammert and Woelk studied the impact of different roughness levels on an axial compressor, which caused a 6–13 % loss in efficiency and up to 30 % loss in overall pressure ratio [3]. Therefore extensive research work has been carried out in order to simulate the surface topography

* Corresponding author. Tel.: +49 511 762 4299; fax: +49 511 762 5115.
E-mail address: Nespor@ifw.uni-hannover.de

doi:10.1016/j.proeng.2011.11.083

under given cutting conditions. The resulting surface topography using ball end mills in 5-axis strategies can be estimated by using analytical equations, which consider the tool diameter, the feed per tooth and the stepover (offset between two cutting paths) [4]. For a more detailed analysis of the topography the cutting tool geometry has to be taken into consideration. This can be realized by analytical generalization of the cutting edge geometry with discretized [5, 6, 7] or solid models of the cutting tool [8]. Bouzakis e.g. segmented the cutting flute into elementary linear sections in order to simulate the surface topography as a function of the tool orientation angles, stepover and feed per tooth [7]. Lui developed two solid models for a ball end mill, which is based on a draft of the flute [8]. The consideration of the cutting edge movement results in a detailed simulation of the surface topography which is a superior approach compared to a Boolean subtraction between workpiece and ball end mill contour. Chen and Huang studied the generation of surface scallops, which is the height of surface peaks due to feed per tooth and stepover, using a simulation which considers cutting edge geometry and movement [9]. They found, that feed per tooth to stepover ratios of about one, lead to scallop heights, which can be 3–4 times higher than the height of the stepover scallops. This high roughness can be reduced by using small tool lead angles of about $\lambda = 10°$. The surface generation model of Arizmendi et al. takes the runout of the ball end mill into account by defining a constant tool parallel axis offset [5]. In their analytical model the equations of cutting edge trajectories and the envelope equations of the material swept by the tool are derived. Benardos and Vosniakos compared current prediction models and classified them into four categories: analytical, empirical, designed experiments and artificial intelligence (AI) approaches [10]. They determine that results produced in recent years are good and the most promising approaches in the future seem to be the analytical and the AI approaches. But combined approaches are still missing and suitable topography models for high accuracy machining are still under investigation. From the literature point of view it can be concluded that the consideration of cutting edge movement and runout is current state of the art to simulate the topography by means of ball end mill. This impeccable topography will be stated as "kinematic topography" in this paper. Most simulation results of the literature agree reasonably well with the experiments, however, stochastic influences are apparent but are not considered yet.

2. Objective and approach of this paper

Most simulated surface parameters in the literature summarized in chapter 1 are underestimated compared to the measured values [7-11]. The main sources of the discrepancies between theoretical and real surface roughness are difficult to isolate, but some reasons are adhesions at the rake-chip interface [11], tool deflection [7], actual tool geometry and stochastic influences. The term "stochastic topography" signifies the difference between kinematic topography and real measured topography.

The objective of this paper is to simulate the kinematic and the stochastic topography by means of ball end milling using a combined approach of an analytical and an empirical surface model. This approach enables the later usage of specific surface parameters, selected in order to their functional significance [12]. Most surface models are only predicting a certain roughness parameter, which might not be sufficient for the technological field of application. Figure 1 shows three surfaces, described by the most common roughness parameters Ra, Rmax and Rz, which are not considering any statistical influences.

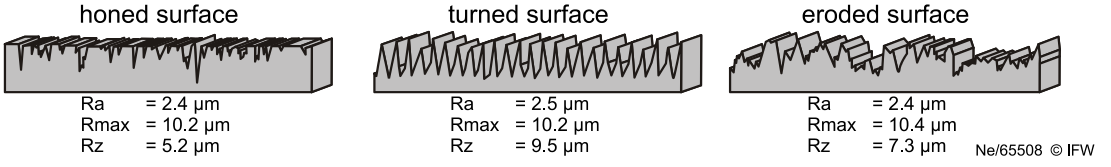

Figure 1: Different roughness profiles with similar arithmetic mean and maximum roughness values [14]

3. Experimental setup and Equipment

All experiments were performed on a 5-axis Deckel Maho DMU125P milling center with a maximum spindle speed of 30,000 min^{-1} and a maximum power of $P_s = 95$ kW. The titanium alloy TiAl6V4 has been chosen as workpiece material due to the wide usage in the compressor stage of modern aircraft engines [13]. In order to exclude the influence of tool wear, indexable inserts of a ball nose endmill cutter have been changed after each experiment. Process forces during machining were measured with a three-component force dynamometer. All experiments of the performed process matrix, which is listed in Table 1, have been repeated once to moderate statistical influences.

The surface topography after machining was measured using a whitelight confocal microscope with a piezo drive and a CCD camera with a vertical resolution of 0.02 µm. To consider all geometric features of the cutting tool, e.g. runout or diameter deviations, the cutting edge and plane surfaces of the inserts have been measured with a Leitz PMM 866 coordinate measuring machine. All multiple X-Y-Z coordinates are imported to a CAD-Software to establish a detailed solid model of the cutting tool.

Table 1: Applied process matrix for the experiments and simulations

	cutting speed v_c [m/min]	feed per tooth f_z [mm]	stepover b_r [mm]	depth of cut a_p [mm]	lead angle λ [°]	tilt angle τ [°]
Range of variations	10 – 80	0.02 – 0.12	0.1 – 0.9	0.2 – 1	15°	0
Number of variations	5	5	5	5	0	0

4. Surface Topography by means of Ball End Milling

4.1. Simulation of kinematic surface topography

The kinematic surface topography has been computed with CutS, a cutting simulation software developed by the IFW. It includes a versatile extension interface to integrate e.g. calculation of cutting forces, detection of geometrical failures during machining or consideration of spindle rotation and machine kinematics within the simulation of material removal [15]. For an appropriate simulation, the previously established CAD-model of the tool was used. The workpiece size complies with the actually measured area of 2.93 x 2.93 mm². To accomplish the Boolean operation of the virtual material removal, the geometrical workpiece model is transferred to a discrete model. In this case a dexel model, as described in [16], was used. The generated dexel map consists of 1024 dexels in each coordinate direction, which is an appropriate value since the lateral resolution of the measurement data amounts to 939 pixels in each direction. To execute the virtual process, an extension was used, which provides a NC-controller interpreting G-Code similar to a machine tool with consideration of the spindle rotation.

For geometrical investigations all parameters, which are significant for the surface generation, such as lead and tilt angle, feed per tooth, stepover and the cutting edge geometry are directly adopted from the real process. For simulation purpose, the kinematic of the process is discretized in time. Therefore, the rotation angle of the indexable insert movement within one time step determines the accuracy of the computed surface. As the course between two angular steps is interpolated as a straight line, the limiting value of the step size is the deviation of the secant. The maximum deviation due to time discretization depends on the tool radius and the applied angular step. It is described as follows:

$$p = r - r * \cos(\alpha/2) \quad (1)$$

For the tool radius of r = 5 mm and an angular step of $\alpha = 3°$, the maximum deviation amounts to 1.71 µm. The distance between the separate dexels counts dx = 2.86 µm, for the used workpiece size. This implies that the maximum deviation of the secant comes to less than the dexel distance. Therefore computational errors can be excluded.

4.2. Determination and evaluation of the stochastic topography

The datasets from the whitelight confocal microscope and the kinematic topography simulation are available as point clouds. To align both datasets to each other, an iterative closest point algorithm (ICP) is applied based on the work of Rusinkiewicz and Levoy [17]. To analyze the difference between both datasets in an arbitrary direction, a plane perpendicular to the X-Y plane can be selected within the algorithm. Figure 2 shows a configuration where the selected planes point towards stepover (1) and feed (2) direction.

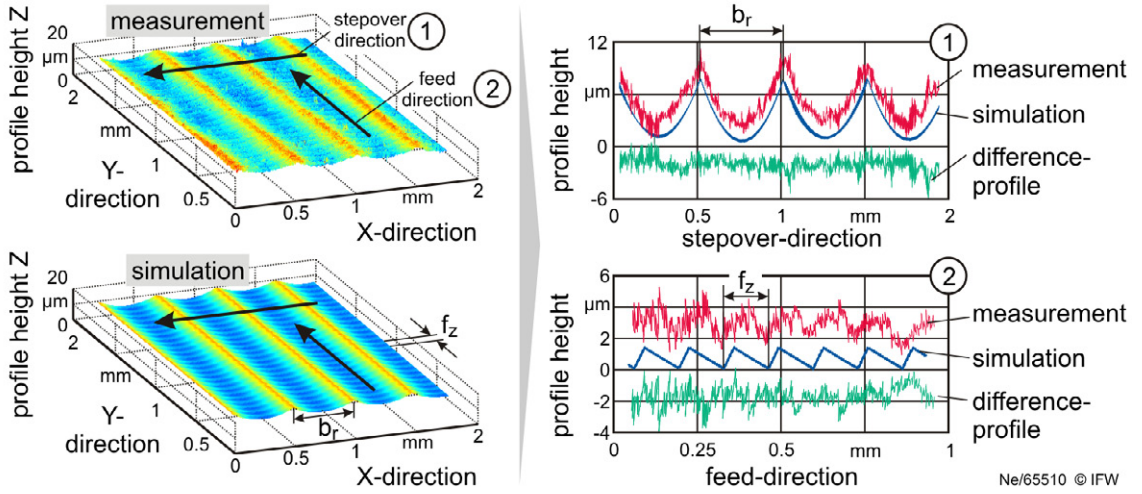

Figure 2: Comparison between measurement and simulation and their differences in feed and stepover direction

In order to compute curves of intersection between the plane and the point clouds, the distance between the plane and each data point is calculated. Only data points within a certain threshold are considered and orthogonally shifted into the plane. After applying a coordinate transformation from 3D to 2D-data, the difference between kinematic roughness and surface measurement can be determined, as depicted on the right side of Figure 2. This so called difference profile has been analyzed for all cutting conditions in feed and stepover direction. The results have shown that the difference profile has recurring characteristics, e.g. a negative average value of the surface height, which is most likely due to tool deflection. The stochastic topography, which is described in the next chapter, is the resulting topography by excluding recurring effects and excluding kinematic topography from the measurements.

4.3. Simulation of stochastic topography

Abbott and Filestone presented a methodology to describe the topography not by a single number, but to consider the irregularities of a surface within a graph [18]. Mathematically the so called Abbott curve is the cumulative probability density function of the surface profile's height. It's most important characteristics are defined in international standards [19]. A straight line divides the Abbott Firestone

Curve into three areas as shown the upper, middle diagram of Figure 3. Valuable parameters are specified from these three areas called Rk (core roughness depth), Rpk (mean height of the peaks protruding from the roughness core profile) and Rvk (mean depth of the valleys protruding from the roughness core profile) with Mr1 and Mr2 as auxiliary parameters.

The Abbott-curve contains probability density data and therefore it will be used for simulating the stochastic topography. Because of the numerous variables depending on the roughness creation phenomena, an empirical model has been chosen for simulating the stochastic topography. The surface topography is highly affected as a result of static and dynamic effects during the cutting process [10]. Therefore the maximum resulting process forces have been used for logarithmic correlation with all five characteristics of the Abbott curve, as shown exemplary for Rk in the upper left of Figure 3.

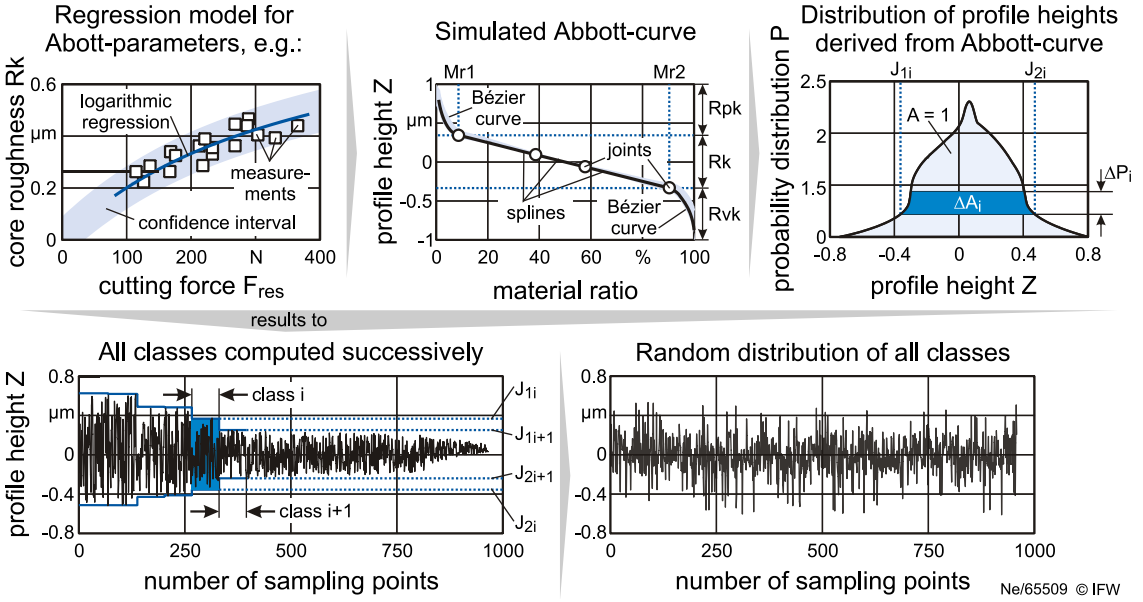

Figure 3: Approach of stochastic topography simulation

The correlations have been realized in feed and stepover direction, which leads to 10 empirical equations for the characteristics of the Abbott curve. By simulating the process forces with given models [20], all characteristics of the Abbott curve can be directly determined. In order to use the probability density data containing in the Abbott-curve, the empirical equations are utilized to simulate the shape of the Abbott curve. Therefore the predicted characteristics are used as joints and interpolation of the core roughness Rk is applied by spline functions whereas peak height Rpk and valley depth Rvk are interpolated by Bézier curves. The result of the simulated Abbott curve is shown in the upper middle diagram of Figure 3. All used joints of this curve are continuously differentiable.

In order to derive the probability distribution of profile heights, the simulated Abbott curve is inversed and normalized. The derivation of the inverse function is the probability distribution P of profile heights, depicted on the upper right diagram of Figure 3. Next the probability distribution P is divided into i horizontal classes with the height ΔP_i, which leads to corresponding expected intervals [J_{1i} J_{2i}] and areas ΔA_i. Distributed pseudo-random numbers are created for each expectation interval, using the algorithm presented in [21]. The amount of generated random numbers for expectation interval is related to the quotient $\Delta A_i/A$. All classes are computed successively to random numbers using their corresponding

expectation interval. The result is shown on the lower left diagram of Figure 3. It can be seen, that the successively computation of all classes results to a step like topography graph due to the different expectation intervals. In order to simulate the stochastic topography all values of the step like topography graph are sampled at random, as shown on the lower right diagram of Figure 3.

4.4. Summation of stochastic and kinematic topography

After the simulation of the stochastic and kinematic topography, both simulations can be added to each other in order to simulate the real surface topography. The result of the summation for a given set of process parameters is shown in Figure 4. The upper left diagram shows the measured profile height in stepover direction and the corresponding simulations on the right side.

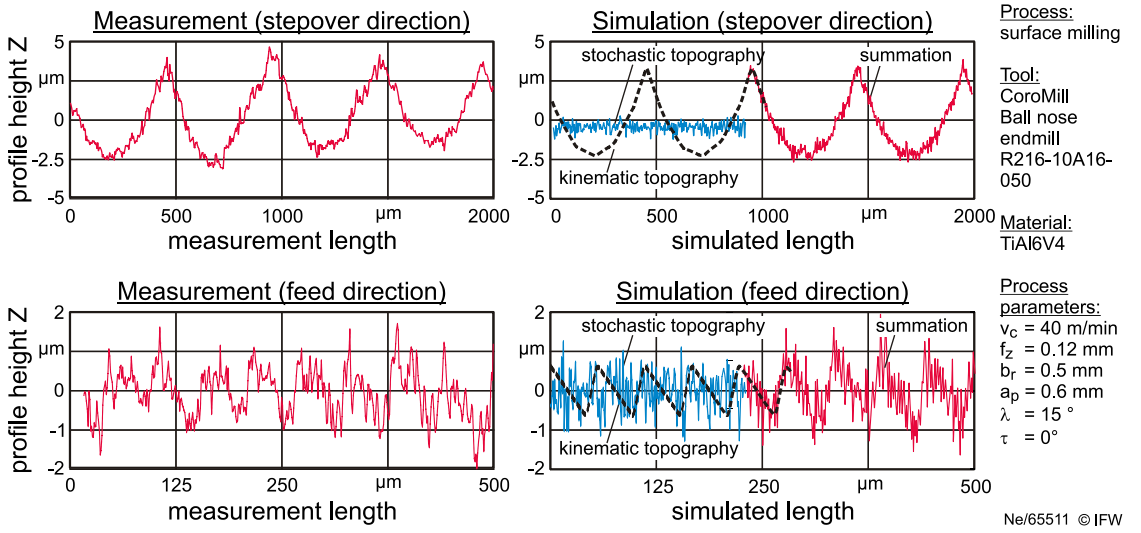

Figure 4: Summation of the simulated kinematic and stochastic topography and comparison to measured values

It can be seen, that the summation of the kinematic and stochastic topography on the right side matches well with the real topography. In this case the influence of the kinematic topography to the summation profile is higher than the stochastic topography due to high values of the stepover b_r. By using a small stepover value of $b_r = 0.1$ mm the influence of the stochastic topography is dominating.

The lower diagrams of Figure 4 show the measured profile height in feed direction and the corresponding simulations on the right side. Compared to the measurements in stepover direction, the stochastic topography has a greater impact to the resulting topography due to the small feed per tooth of $f_z = 0.12$ mm. Using even smaller feeds, the influence of the kinematic roughness further decreases.

The average difference for all sets of process parameters between the kinematic roughness and the measurements is 19.4 % for Rz and 32.9% for Ra. With the usage of the combined model the average difference has been reduced to 6.7 % for Rz and 5.5 % for Ra.

5. Conclusion and Outlook

The term “Surface Integrity” can be classified into topography characteristics and surface layer characteristics. Due to the crucial influence on the functional behavior, the surface topography is usually the most important feature of complex high performance parts. Therefore an innovative combined method

for predicting the topography by means of ball end milling is developed, which computes the kinematic topography by a dexel model as well as the statistical influences by an empirical model. Within the proposed method the simulated topography shows a good similarity to the measured one. For more general usage in the future this method will be evolved for 3D-stochastic topography and will also consider other characteristics of the difference profile.

Acknowledgements

The authors thank the German Research Foundation (DFG) for the financial support within the Collaborative Research Center 871: Refurbishment of complex capital goods.

References

[1] Bons JP. A Review of Surface Roughness Effects in Gas Turbines. J. Turbomach. 2010;132-2, 021004 (16 pages)
[2] Klocke F, Feldhaus B, Mader S.Development of an incremental rolling process for the production of defined riblet surface structures. Prod Eng Res Devel 2007;1, p. 233–237. DOI 10.1007/s11740-007-0031-y
[3] Bammert K, Woelk GV. The Influence of the Blading Surface Roughness on the Aerodynamic Behavior and Characteristics of an Axial Compressor. ASME J Eng Power 1980; 102
[4] Ozturk E, Tunc LT., Budak E. Investigation of lead and tilt angle effects in 5-axis ball-end milling processes. Intl. J of Machine Tools & Manufacture 2009; 49, p. 1053–1062
[5] Arizmendi M et al. Model development for the prediction of surface topography generated by ball-end mills taking into account the tool parallel axis offset. Experimental validation. CIRP Annals - Manufacturing Technology 2008; 57, p. 101–104
[6] Gao T, Zhang W, Qiu K, Wan M. Numerical Simulation of Machined Surface Topography and Roughness in Milling Process. J. Manuf. Sci. Eng 2006; 128, p. 96–104
[7] Bouzakis KD, Aichouh P, Efstathiou K. Determination of the chip geometry, cutting force and roughness in free form surfaces finishing milling, with ball end tools. Intl. J of Machine Tools & Manufacture 2003; 43, p. 499–514
[8] Liu N, Loftus M, Whitten A. Surface finish visualisation in high speed, ball nose milling applications. Intl. J of Machine Tools & Manufacture 2005; 45, p.1152–1161
[9] Chen JS, Huang YK, Chen MS. A study of the surface scallop generating mechanism in the ball-end milling process. Intl. J of Machine Tools & Manufacture 2005; 45, p.1077–1084
[10] Benardos PG, Vosniakos GC. Predicting surface roughness in machining: a review. Intl. J of Machine Tools & Manufacture 2003; 43, p.833–844
[11] Grzesik W. A revised model for predicting surface roughness in turning. Wear 1996; 194, p.143–148
[12] Whitehousea DJ. The parameter rash - is there a cure? Wear 1982; 83, p. 75–78
[13] Neugebauer R, et al. Manufacture of titanium hollow shaft by incremental forming. Prod Eng Res Devel 2011; 5, p. 227–232
[14] Raimund V. Rauheitsmessung Theorie und Praxis, 1st ed. München, Beuth Verlag GmbH; 2005
[15] Denkena B, Böß V. Technological NC Simulation for Grinding and Cutting Processes Using CutS. In: Proceedings of the 12th CIRP Conference on Modelling of Machining Operations May 7-8, 2009. Donostia-San Sebastián, Spain, p. 563–566
[16] Van Hook T. Real Time Shaded NC-Milling Display. Computer Graphics Proceedings 1986; 20, p. 15–20
[17] Rusinkiewicz S, Levoy M. Efficient Variants of the ICP Algorithm. In Proceedings of the 3rd Intl. Conf. on 3D Digital Imaging and Modeling, Quebec City: 2001, p.145–152
[18] Abbott EJ, Firestone FA. Specifying surface quality: a method based on accurate measurement and comparison, Mech Eng 1933; 55, p.569–572
[19] DIN EN ISO 13565-2. Geometrical Product Specifications - Surface texture: Profile method - Surfaces having stratified functional properties - Part 2: Height characterization using the linear material ratio curve, 1996
[20] Altintaş Y, Roukema JC. Mechanics and dynamics of general milling cutters. Part I: helical end mills. Intl. J of Machine Tools & Manufacture 2001;41, p. 2195–2212
[21] Matsumoto M, Nishimura T. Mersenne Twister: A 623-Dimensionally Equidistributed Uniform Pseudorandom Number Generator. ACM Transactions on Modeling and Computer Simulation 1998;8, p. 3–30